Ultrafine Aerosol Emission from the Free Fall of TiO_2 and SiO_2 Nanopowders †

N. Ibaseta and B. Biscans*
Laboratoire de Génie Chimique UMR CNRS 5503[1]

Abstract

Due to the increasing production and development of nanoparticles, it has become necessary to control the exposure to ultrafine particles when handling nanopowders. The use of dustiness tests makes it possible to compare the ability of a given powder to re-suspend particles, and to determine the effect of the different external (powder handling method) or internal parameters (powder properties). A dustiness test associated with an electrical low-pressure impactor (ELPI) device is proposed to study the free fall of nanopowders. Titanium dioxide (TiO2) and fumed silica (SiO2) are the studied nanopowders. The free falling of nanopowders in the test chamber generates bimodal aerosols corresponding to the re-suspension of the micrometric agglomerates that constitute the nanopowders and to the breakage and/or erosion of these agglomerates leading to ultrafine aggregates. The presence of ultrafine aggregates was checked by scanning electron microscopy (SEM). When the height of fall and the dropped mass of the powders are increased, the aerosol concentration increases. Aerosols are mostly generated by the impact of nanopowders on the floor of the experimental chamber. Fumed silica is dustier than titanium dioxide, and its agglomerates break more easily.

Keywords: Nanopowder, Aerosol, Free-Falling powder, ELPI, Dustiness

1. Introduction

Nanoparticles, also called ultrafine particles, are defined as particles smaller than 100 nm. Their high surface-to-volume ratio gives them interesting properties: magnetic, mechanical, electrical, optical, thermodynamical and thermal properties that are different from those of the source materials[1)]. They thus constitute an enhanced development, due to the wide range of applications in electronics, biomedicine, pharmaceutics, cosmetics, catalysts and materials[2)]. This increasing interest in nanomaterials has led to some questions about the possible adverse effects on human health[2-4)]. Previous works have studied the toxicity of ultrafine particles. Their conclusions can be summarized as follows in a non-exhaustive way:

- Ultrafine particles induce much higher lung inflammation than an equal mass of larger respirable particles of the same material[5)].
- Lung damages due to agglomerates and aggregates of nanoparticles (henceforth called nanostructured particles) is more severe than that caused by particles lacking a nanostructure, even when they have the same size[4)].
- Ultrafine particles can pass into the bloodstream[6)].
- Pulmonary inflammation due to low-solubility nanostructured particles is fairly independent of particle compositions and sizes. On the contrary, it correlates closely with surface area concentration[3)].
- Particle shape should be taken into account when studying the hazards; anisotropic particles such as fibres or nanotubes enhance pulmonary damage[4)].
- Surface chemistry can modify particle toxicity; for instance, the inflammation response caused by quartz can be strongly reduced by modifying the

surface of the particles (e.g. with aluminium lactate)[7].

All those studies point out that it is necessary to determine the exposure levels during manufacturing, handling and clean-up operations with nanopowders. Not only nanoparticles, but nanostructured particles as well as aerosolised liquid suspensions containing nanoparticles should be taken into account. Several parameters such as particle shape, size and surface area of the nanostructured particles are properties which should be determined.

Two different approaches can be followed. The first one concerns measurement of the exposure levels at work sites in order to obtain representative values of real industrial levels. However, it is difficult in that case to identify the parameters inducing ultrafine dust generation, as well as their influence. A good summary of this kind of approach can be found in Aitken *et al* [2].

The other approach concerns dustiness tests applied to nanostructured powders. Dustiness is defined as the trend of a given material to generate dust. In such tests, a powder is subjected to different constraints such as free falling, fluidisation or stirring in a rotating drum[8]. Although the values obtained are less representative than measurements at work sites, the identification of key parameters affecting dust emission becomes easier.

To our knowledge, the only previous studies using dustiness tests for nanomaterials were implemented with single-walled carbon nanotubes (SWCN)[9, 10] and fumed silica[11]. Tests with SWCN were carried out in a test tube agitated by a vortex shaker. The emitted aerosol size distribution was measured by two scanning mobility particle sizers, SMPS[12], and an aerodynamic particle sizer, APS[13]. The aerosol concentration was found to be quite low and ultrafine particles were not significantly detected, except when applying strong agitation. These results were checked against field measurements where the overall airborne concentration of nanotubes was estimated to be quite low (lower than $53\mu g/m^3$).

Tests with fumed silica were carried out in a rotating drum[8] and in a dropping test (Dust View[11], from Palas society). Size distributions were not measured in that work. For the rotating drum test, a dustiness index was defined as the mass ratio of the emitted ultrafine aerosol (sucked and collected by a filter) to the initial nanostructured powder. For the dropping test, the characteristic values used were the maximum light extinction of a laser beam placed next to the settling dust stream, as well as the light extinction 30 seconds after the fall of the powder.

The aim of the present work is to design an experimental set-up which enables the study of ultrafine dust generation by free-falling nanostructured powders. The results of the test provide the size distribution and the mass concentration of the aerosol. This experiment will therefore make it possible to check the presence (or absence) of ultrafine particles suspended in air due to free-falling powders, and to study the effect of parameters such as the drop height or the dropped mass of powder on both size distribution and concentration. Such an experiment can provide a tool to quantify and to compare the ability of several nanostructured powders to generate ultrafine aerosols for a given situation (free falling). It can also help to correlate the properties of the particles to their behaviour.

2. Experimental Methods

2.1 Experimental set-up

The experimental set-up shown in **Fig. 1** is inspired by the MRI test [14]. Powder fall was performed in a stainless steel chamber with internal dimensions $180 \times 50 \times 80$cm. The front and lateral

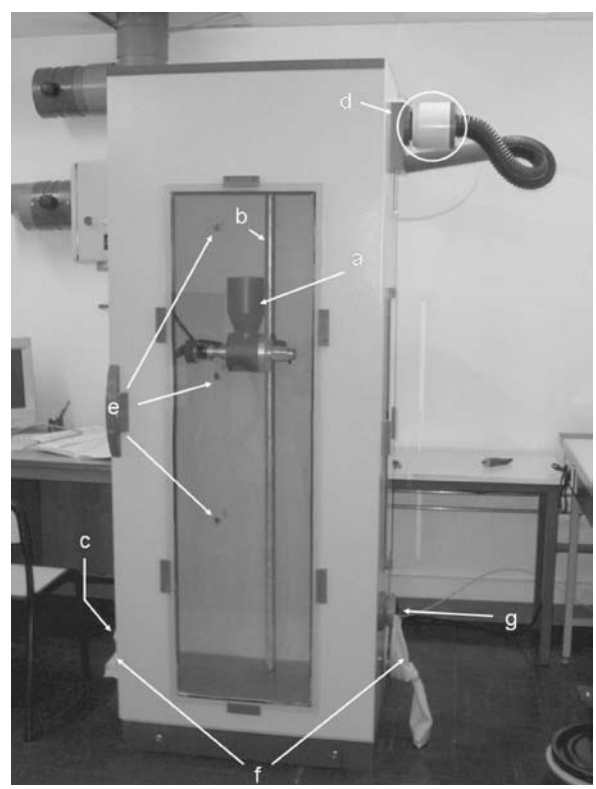

Fig. 1 Free-falling nanostructured powders device for aerosol emission measurement: (a) silo; (b) supporting stem; (c) inlet HEPA filter; (d) outlet HEPA filter; (e) sampling point; (f) latex gloves; (g) vacuum cleaner inlet.

sides of the chamber are partially of glass to enhance visualization. The powder is stocked in a silo (a) which can be adjusted in height inside the chamber along a supporting stem (b). The silo comprises a storage vessel that tapers into a beaker of 125cm^3. The beaker is connected to a rotating system so that two positions are possible: filling and emptying. A pneumatic vibrator is added to the system in order to help both operations.

Six aerosol extraction positions (e) connected to an electrical low-pressure impactor (ELPI) are placed on both sides at 50, 100 and 150 cm from the bottom of the chamber. Both air inlet (c) and outlet (d) holes were placed at the left and the right side of the chamber, respectively. Two high-efficiency particulate air (HEPA) filters are used in order to clean the air entering and exiting the chamber. Cleaning is carried out by a vacuum cleaner (g) handled by means of two latex gloves (f) placed on both sides.

Three sets of experiments were carried out. The first one concerned video recording of the powder fall. Recording was carried out with a Photron FASTCAM-APX camera. The resolution, the frame rate and the shutter speed were fixed at 1024×1024 pixels, 1000 fps and 1/2000 s, respectively. Since the front door of the chamber was not entirely transparent, video recording was accomplished by elevating the impact surface. Hence, the maximum height of fall in the video-recorded experiments was 130cm, and not 160cm as in the other experiments presented in the next sections.

The second set of experiments consisted of measuring the aerosol concentration and size distribution after a powder fall. The aerosol concentration and size distribution were measured by an electrical low-pressure impactor (ELPI). The ELPI device enables the particles contained in the aerosol to be separated according to their size, and to determine the particle concentration corresponding to each class. The principle of the ELPI measurements is explained in the next section.

These experiments were started by placing the nanostructured powder in the silo, closing the front door and switching on the air extraction through the HEPA outlet filter. The HEPA filter placed at the air inlet allowed the particle concentration (coming from the atmosphere) in the chamber to be decreased. At the same time, the ELPI was switched on to equilibrate the temperature in the chamber. After a stabilisation time of at least 20-30 minutes, the air extraction was switched off and the clean air evolution was recorded during 15-20 minutes. The beaker was then turned upside down and the powder fell in the chamber.

The dropped mass of powder can be changed by partially filling the beaker below the silo. In that case, the mass of powder was weighed before placing it in the beaker. Another possibility was to totally fill the beaker. In that case, the method of filling was more reproducible, but the dropped mass of powder was not directly measured before each experiment. It was obtained for each powder by carrying out preliminary experiments, recovering the dropped powder in a plastic bag and weighing the bag.

Finally, a third set of experiments were carried out in order to validate the presence of ultrafine aggregates in the emitted aerosol by scanning electron microscopy (SEM) visualisation of the particles collected on the ELPI stages. These SEM visualisations need specific experiments. They were performed for a given height of fall, fixed at 160 cm, and a given height of sampling: 50 cm.

2.2 Principle of the ELPI measurements

The ELPI[15-22] is a device able to measure aerosol concentration as well as size distribution of the aerosol in the range between 30 nm and 10μm at a given location. The principle of the instrument has been well explained elsewhere[15-18], so that the main elements needed for this work will only be touched upon here.

A schematical view of the ELPI device is shown in **Fig. 2**. The aerosol is sucked by a vacuum pump. It

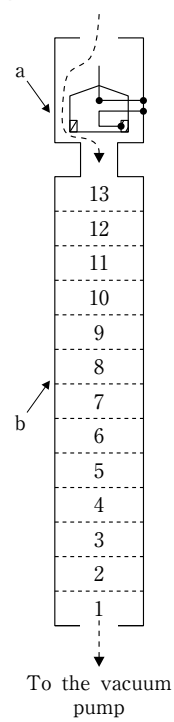

Fig. 2 Schematical representation of the Electric Low-Pressure Impactor (ELPI) used in this study: (a): corona charger; (b): cascade impactor.

goes first through a corona charger (a), where particles are charged positively depending on their mobility diameter. The mobility diameter (d_b) is defined as the diameter of the sphere having the same mobility, i.e. the same velocity-to-driving force ratio as the particle. Since, according to the Stokes-Einstein equation, the particle diffusion coefficient is proportional to the particle mobility[23], the mobility diameter is the most representative diameter when describing Brownian motion.

The cascade impactor (b) is located downstream of the corona charger. It classifies the particles according to their aerodynamic diameter. The aerodynamic diameter (d_a) is defined as the diameter of the sphere with a unit density of 1000kg/m^3 having the same settling velocity as the particle. This diameter is the key particle property for characterising respiratory deposition[23].

When the particles are collected on an ELPI stage, they generate an electrical current that is measured by the electrometers. Teflon insulators are placed between the ELPI stages in order to isolate the stages electrically.

As the particle charge depends on the mobility diameter and the particle deposition on the ELPI stages depends on the aerodynamic diameter, the conversion between both diameters is essential. If the particles are spherical, the diameters are related through equation 1, where ρ_p is the particle density, ρ_0 = 1000kg/m^3 and C_C is the slip (or Cunningham) correction factor[23]. The aerodynamic diameters and their corresponding mobility diameters were calculated in Table 1 for the two different particle densities used in this work. If the particle density is 1000kg/m^3, then the aerodynamic diameter and the mobility diameter have the same values.

$$\rho_p d_b^2 C_C(d_b) = \rho_0 d_a^2 C_C(d_a) \quad (1)$$

Measurement data can be treated by ELPI software[17, 19], which converts raw current data into aerosol concentration and size distribution. The only required parameters are the particle density and the calibration data. Both the charger and the cascade impactor calibrations are performed by the manufacturer[16]. Cascade impactor calibration provides the cut-off aerodynamic diameters of the ELPI stages. Charger calibration provides the charger efficiency (E_{ch}) as a function of the mobility diameter. The charger efficiency represents the current carried by charged particles of a given size leaving the charger, divided by the particle number concentration in the aerosol.

For each stage, ELPI software calculates the average aerodynamic diameter given by the geometric mean of the cut-off diameters of a given stage and the previous one. Then the mobility diameter is calculated by Eq.(1). The charger efficiency is then calculated according to its calibration data. Finally, the particle number concentration is given by the ratio between the current I' and the charger efficiency E_{ch}:

$$N = \frac{I'}{E_{ch}} \quad (2)$$

I' is not the measured current I, but a corrected current[17] that takes into account the fine particle losses in upper ELPI stages[20, 21]. The rebound of the particles impacting against an ELPI stage is minimised by greasing the ELPI substrates with Vaseline.

Table 1 Mean aerodynamic diameters of ELPI stages, and their equivalent mobility diameters

ELPI stage	d_a (ρ_0=1000 kg/m^3)	d_b (ρ_p=2300 kg/m^3)	d_b (ρ_p=3100 kg/m^3)
1	38.3 nm	17.6 nm	13.2 nm
2	70.9 nm	34.1 nm	25.8 nm
3	119 nm	60.5 nm	46.6 nm
4	199 nm	108 nm	85.3 nm
5	312 nm	180 nm	146 nm
6	477 nm	289 nm	239 nm
7	753 nm	471 nm	396 nm
8	1.21 μm	777 nm	660 nm
9	1.93 μm	1.25 μm	1.07 μm
10	3.05 μm	2.01 μm	1.70 μm
11	5.11 μm	3.37 μm	2.90 μm
12	8.05 μm	5.31 μm	4.57 μm

2.3 Tested nanostructured powders

Two types of nanostructured powders were selected for testing the device: titanium dioxide, TiO_2 (G5, produced by Millenium Inorganic Chemicals) and fumed silica, SiO_2 (Aerosil 200, produced by Degussa). Although both powders are formed by microscopic agglomerates of nanoparticles, their structures are quite different, as can be seen on the SEM photographs (**Fig. 3**). TiO_2 agglomerates (**Fig. 3.a**) have a compact (raspberry-like) structure; whereas SiO_2 agglomerates (**Fig. 3.b**) resemble a foam with a high air content.

The main physical properties of both powders were measured and reported in **Table 2**. Agglomerate size measurements were performed by laser diffraction (Mastersizer 2000, Malvern Instruments). The difference between mass and number median diameters can be explained by the fact that for one given large particle, several fine particles are needed to obtain its weight. Primary particle sizes are provided by the manufacturers and are in agreement with our transmission electron microscopy (TEM) visualisations (same range of sizes). Particle densities were measured by helium picnometry, whereas tapped densities were obtained using a Hosokawa Micron Powder Characteristics Tester. Finally, the bulk density was calculated from the dropped mass of powder measured when the beaker was completely filled (the beaker volume is $125cm^3$).

3. Results

3.1 Video recording of the powder fall

In order to analyse the two sources of the aerosols: dust generation from the particles falling and dust generation after impaction on the chamber floor, the free-fall process was visualised by video camera recording. The same volume of dropping powder and same height of fall (130cm) were used for both powders TiO_2 and SiO_2. Several pictures were taken

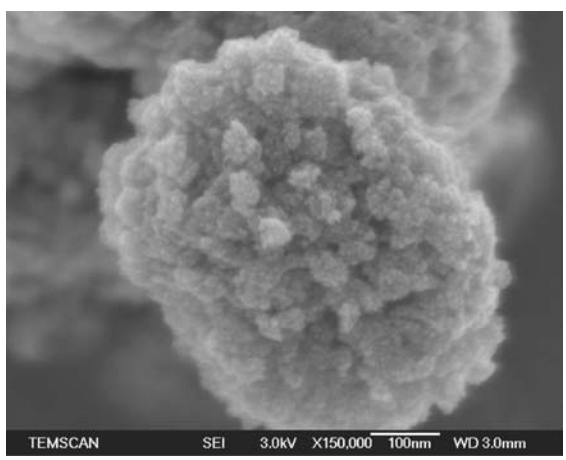

Fig. 3a Titanium dioxide (TiO_2).

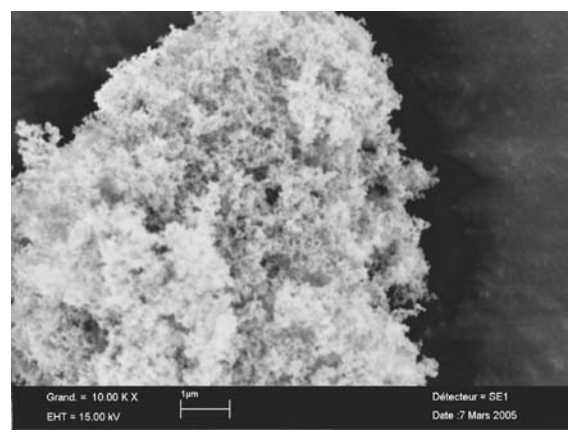

Fig. 3b Fumed silica (SiO_2).

Fig. 3 SEM photographs of the nanostructured powders.

Table 2 Specific properties of the nanostructured powders used in the free-fall test

	TiO_2	SiO_2
Primary particle size (provided by the manufacturer, checked by TEM)	5-12 nm	12 nm
Agglomerate mass median diameter (measured by laser diffraction)	1.3 μm	10 μm
Agglomerate number median diameter (measured by laser diffraction)	0.80 μm	5.2 μm
Particle density (measured by helium picnometry)	3100 kg/m^3	2300 kg/m^3
Tapped density (measured by a Hosokawa Micron Powder Characteristics Tester)	620 kg/m^3	58 kg/m^3
Bulk density (calculated as described in the text)	370 kg/m^3	44 kg/m^3
BET surface area	320 m^2/g	190 m^2/g
Crystalline structure (given by the manufacturer)	Anatase	Amorphous

during the fall: they show that for both powders, the column of the falling powder is neither regular in shape nor in particle concentration. Moreover, when the first particles reach the floor of the chamber, others are still leaving the beaker in the upper part of the chamber. The mean time of the fall, considered as the time during which there was some powder falling from the silo, was found to be less than 2 s for TiO_2 and around 9 s for SiO_2.

For TiO_2, the particle cluster impacts on the surface of the chamber floor and generates smaller agglomerates. Oblique jets are observed when the powder impacts on a layer of particles previously fallen. These jets can lead to particle re-suspension. **Fig. 4** is a view of the impact of TiO_2 powder, showing the rising jets.

For SiO_2 powder, the impact shown in **Fig. 5** is different: the small agglomerates seem to bounce on the surface and horizontal air/particle clouds are generated parallel to the surface.

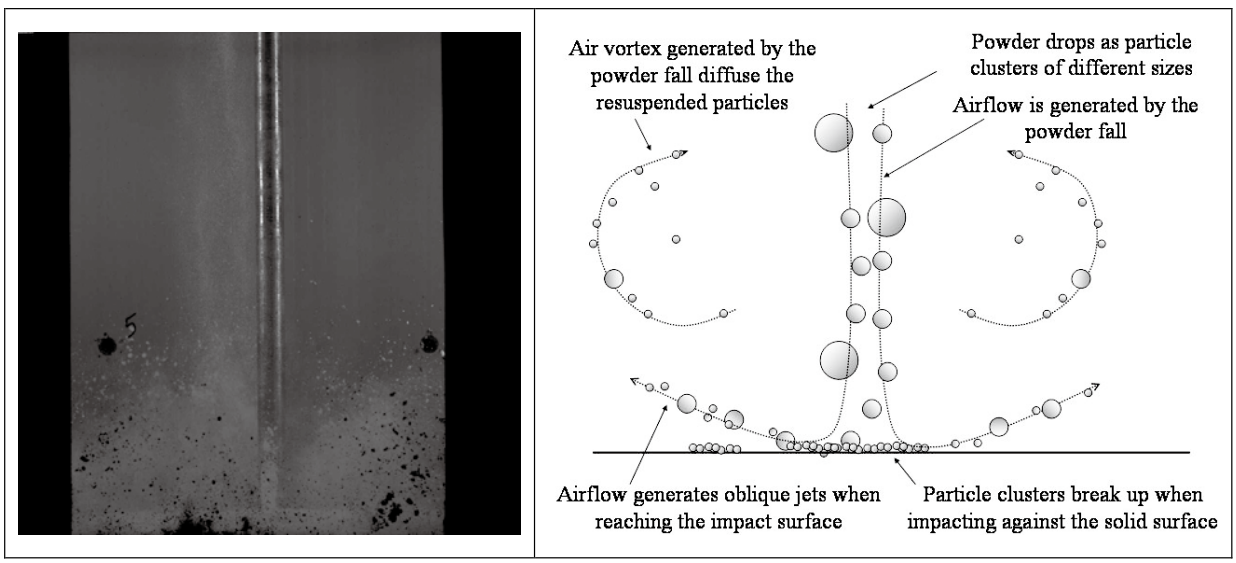

Fig. 4a Camera visualisation

Fig. 4b Schematic representation of the fall

Fig. 4 TiO_2 nanopowder fall.

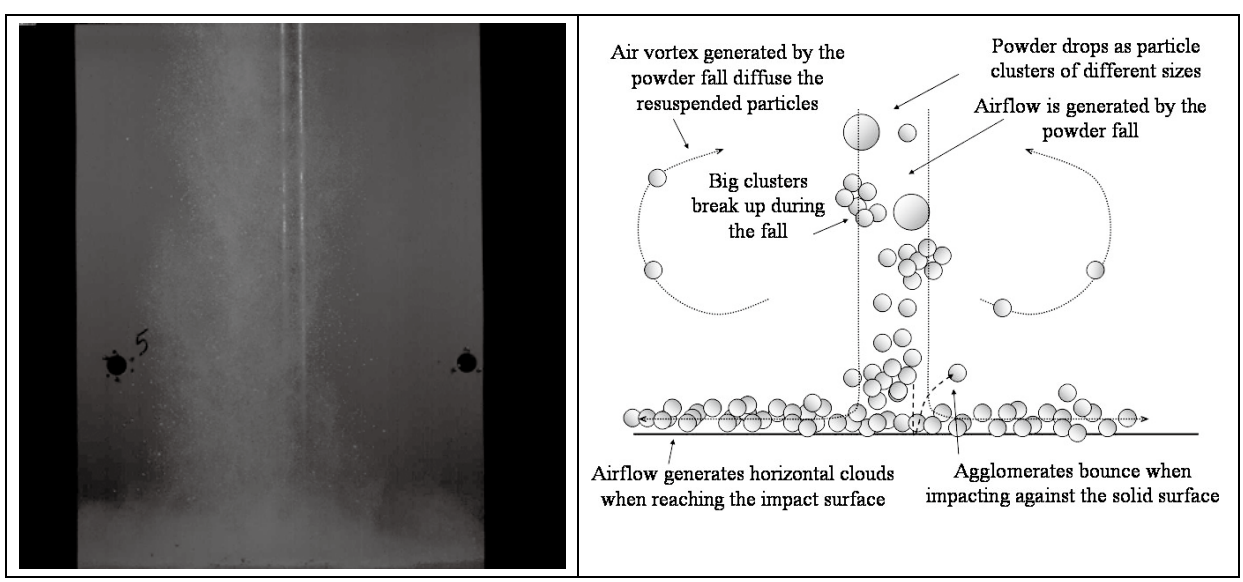

Fig. 5a Camera visualisation

Fig. 5b Schematic representation of the fall

Fig. 5 SiO_2 nanopowder fall.

Finally, in both cases, particles are re-suspended after the impact and rise along the walls of the chamber. Consequently, the measurements performed on the aerosol with the ELPI instrument correspond to the added contributions of the dust generated from the fall and the dust generated from impact.

3.2 Time evolution of the aerosol

The experimental conditions of the quantitative tests performed in the dustiness experimental set-up are reported in **Table 3**.

Although ELPI raw currents are measured in a continuous way, the results are averaged over at least 5 consecutive seconds[18] because of the different residence times of the particles in the cascade impactor. This time (5 seconds) compared with the time of fall (2 s for TiO_2 and 9 s for SiO_2) shows that the aerosol generation during the free fall and the aerosol generation due to impact cannot be distinguished by ELPI measurements.

Fig.s 6.a and **6.b** show the time evolution of the raw currents measured on ELPI stages during the free fall of TiO_2 and SiO_2 nanopowders, respectively, the first one corresponding to experiment E2.5 and the second one to E1.5. For both powders, when sampling near the impact surface, the aerosol concentration increases rapidly and then decreases faster than an exponential law. This is due to both settling and convection by the air vortex generated by the powder fall[24].

After some 10-15 minutes, aerosol concentration (which is proportional to the measured currents) decreases following an exponential law. This is typical of stirred settling[23].

For SiO_2 (**Fig. 6.b**), the fluctuations are much more significant, giving way to two independent peaks. When the second peak is reached, the aerosol concentration decreases in an exponential way. This decrease is faster than for TiO_2, since SiO_2 particles settle faster than the TiO_2 ones because of their larger aerodynamic diameter (see next section).

In the following sections, the results (size distribu-

Table 3 Operating conditions of the experiments performed in the free-falling powder chamber

Experiment number	Powder	Height of fall	Height of sampling	Dropped mass		Temperature	Humidity
E1	SiO_2	160 cm	50 cm	5.5 ± 0.2 g	E1.1	23.6℃	52.2%
					E1.2	22.8℃	60.8%
					E1.3	23.1℃	56.3%
					E1.4	25.1℃	49.1%
					E1.5	24.5℃	48.4%
E3	SiO_2	120 cm	50 cm	5.5 ± 0.2 g	E3.1	26.1℃	56.6%
					E3.2	23.4℃	65.2%
E4	SiO_2	80 cm	50 cm	5.5 ± 0.2 g	E4.1	26.0℃	58.7%
E5	SiO_2	50 cm	50 cm	5.5 ± 0.2 g	E5.1	22.0℃	52.3%
					E5.2	23.7℃	53.4 %
					E5.3	22.8℃	60.0%
E2	TiO_2	160 cm	50 cm	45.9 ± 0.9 g	E2.1	19.3℃	40.3%
					E2.2	22.5℃	39.1%
					E2.3	20.5℃	40.9%
					E2.4	23.1℃	37.9%
					E2.5	20.5℃	48.0%
E6	TiO_2	120 cm	50 cm	45.9 ± 0.9 g	E6.1	23.7℃	55.8%
E7	TiO_2	80 cm	50 cm	45.9 ± 0.9 g	E7.1	24.2℃	47.1%
E8	TiO_2	50 cm	50 cm	45.9 ± 0.9 g	E8.1	22.7℃	47.3%
E9	TiO_2	160 cm	100 cm	45.9 ± 0.9 g	E9.1	24.8℃	58.8%
E10	TiO_2	160 cm	150 cm	45.9 ± 0.9 g	E10.1	20.6℃	57.8%
E11	TiO_2	160 cm	50 cm	5.5 g	E11.1	23.2℃	61.1%
				5.5 g	E11.2	25.0℃	50.7%
E12	TiO_2	120 cm	50 cm	5.5 g	E12.1	23.6℃	57.3%
E13	TiO_2	80 cm	50 cm	5.5 g	E13.1	24.0℃	54.0%

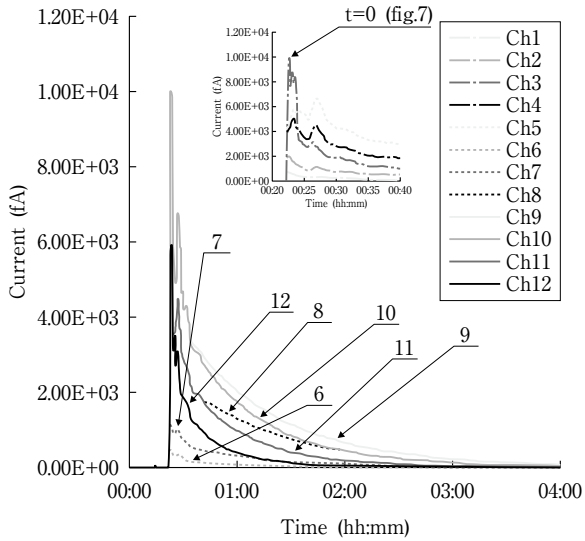

Fig. 6a Experiment E2.5.

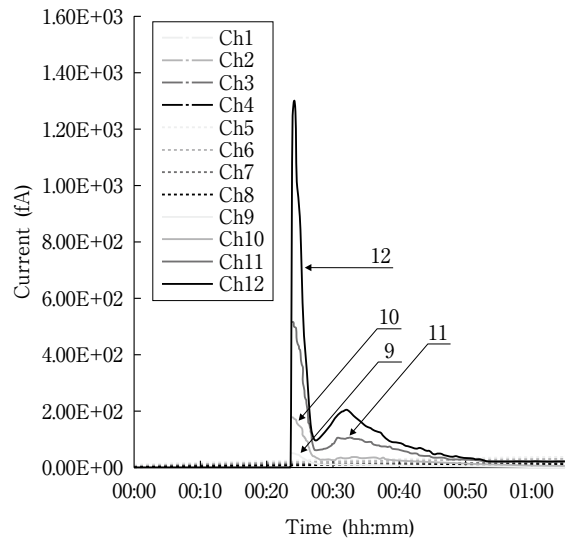

Fig. 6b Experiment E1.5.

Fig. 6 Time evolution of ELPI raw currents during the free fall of nanopowders

tion and particle concentration) were obtained by considering the maximum of the first peak of the current curve. In order to reduce the drift effect, the currents obtained just before the peak were subtracted from the measured currents.

Aerosol concentration at higher sampling positions (100cm and 150cm) increases more slowly, and begins to decrease following an exponential law. This behaviour can be explained by the fact that the main part of the aerosol is generated during the impact against the solid surface, and then diffuses (by Brownian and especially by hydrodynamic diffusion) to higher positions. Once the aerosol concentration is uniform in the chamber, only settling becomes important. This can be verified in **Fig. 7**, which shows the particle concentration at different sampling positions for different times. At t=0 (which corresponds to the first peak), the aerosol is much more concentrated near the impact surface (since most of the aerosol is generated during the impact). Aerosol concentration near the surface decreases rapidly, whereas concentration at higher sampling positions increases.

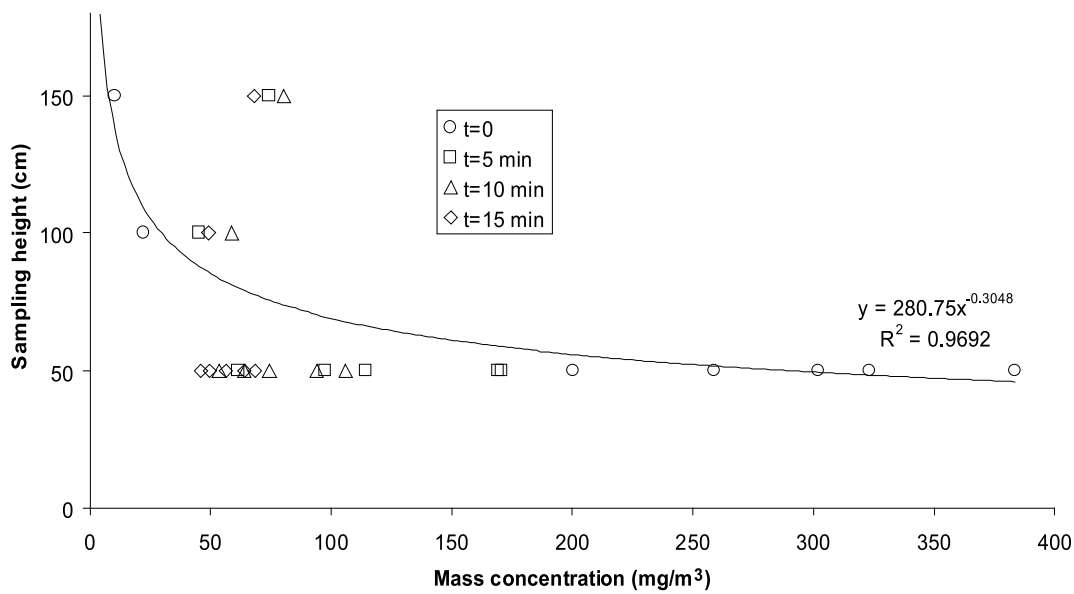

Fig. 7 Time evolution of the aerosol mass concentration at different sampling positions (t=0 corresponding to current maximum). Experiments E2, E9 and E10.

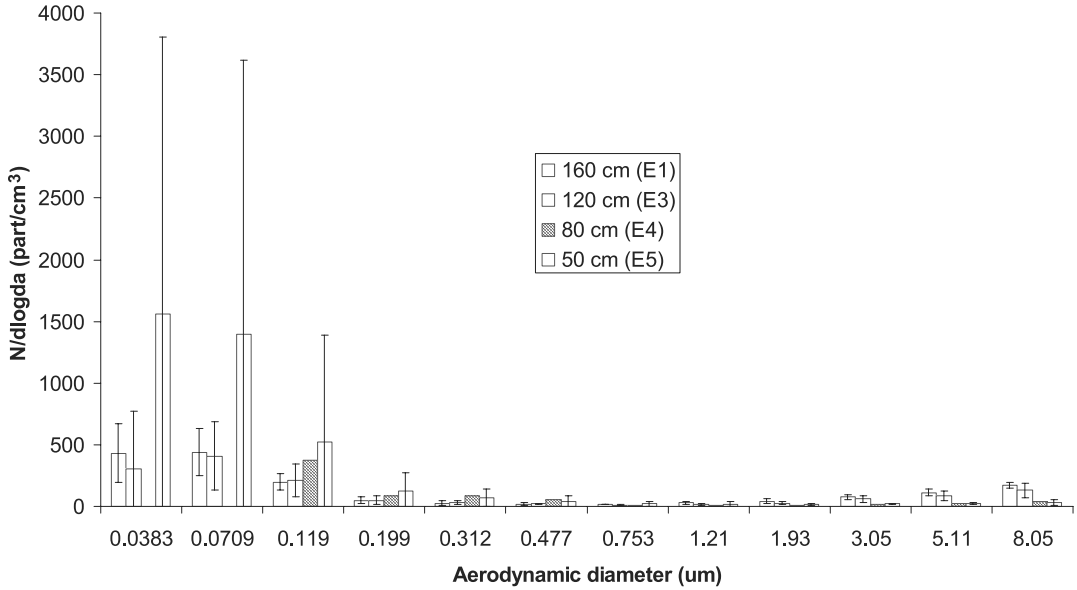

Fig. 8a SiO_2 (experiments E1, E3 to E5).

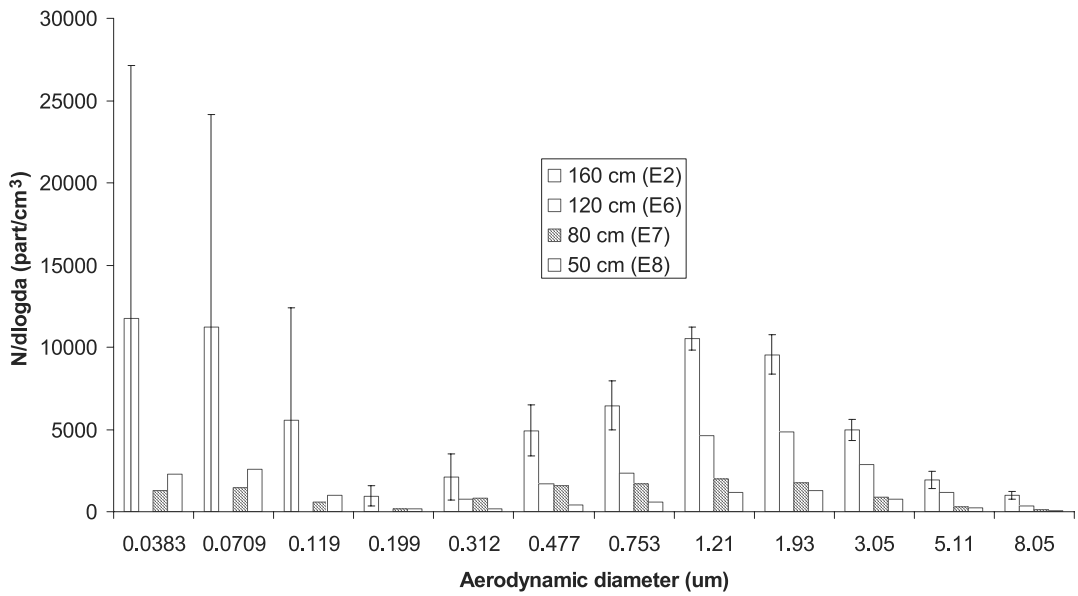

Fig. 8b TiO_2 (experiments E2, E6 to E8).

Fig. 8 Number size distribution of the generated aerosols at different heights of fall

At t=10 min, aerosol concentration is uniform in the chamber. At t=15 min, aerosol concentration begins to decrease homogeneously in the entire chamber.

3.3 Characterisation of the emitted aerosol

3.3.1 Size distribution

Fig. 8 shows the size distribution of the aerosols obtained in experiments E1 to E8, corresponding to different heights of fall at the same sampling position. **Fig. 9** shows the size distribution of the aerosols in experiments E2, E9 and E10, corresponding to different sampling heights for a same height of fall. Error bars represent the confidence interval for a confidence level of 95%. In all cases, the size distributions show two maxima, one corresponding to ultrafine particles, the other one to micrometric particles. The maximum corresponding to micrometric particles is located on the 12^{th} ELPI stage for SiO_2 and on the 8^{th} stage for TiO_2. They correspond to aerodynamic diameters of 8.05μm and 1.21μm, respectively. If particle sizes are expressed as mobility diameters, they are equal to 4.57μm for SiO_2 and 0.660μm for TiO_2. They are in good agreement with the number median diameters of the initial powders, measured by light

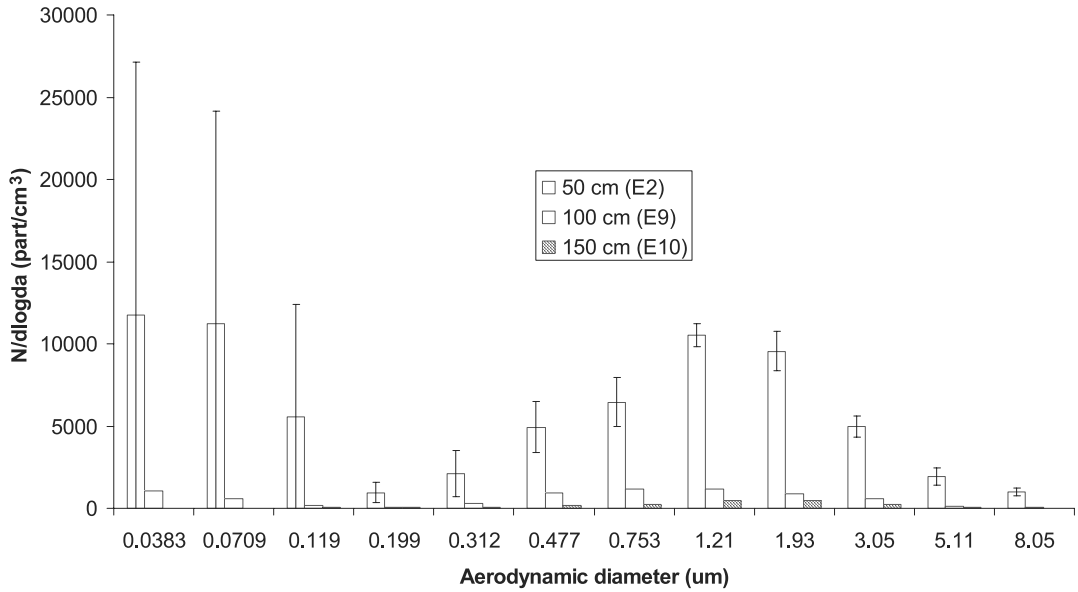

Fig. 9 Number size distribution of the generated aerosols at different sampling heights, for TiO_2 nanopowder (experiments E2, E9 and E10).

scattering, which are equal to 5.2μm for SiO_2 and 0.800μm for TiO_2. Hence, these maxima correspond to the re-suspension of the particles just in the same state as they are in the powder.

The ultrafine maximum is located in the 1st or the 2nd ELPI stages, showing the presence of primary particles or at least ultrafine aggregates in the aerosol. This fact has been checked by visualisation of the particles collected on the ELPI stages by a scanning electron microscope (SEM), Section 3.3.2.

In order to analyse the reproducibility of the measurements, experiments E1 and E2 were repeated 5 times and reproducibility was defined as the average of the ratio between the standard deviation and the averages of the particle number concentration for each stage (Eq. (3)).

$$\text{Reproducibility} = (1/12) \cdot \sum_{i=1}^{12} (\sigma_i / \overline{x}_i) \qquad (3)$$

The calculated reproducibility values are 0.47 for E1 and 0.62 for E2. The maximum corresponding to micrometric particles is reproducible for both powders $(\sigma/\bar{x})_{12}$=0.16 for E1, $(\sigma/\bar{x})_8$=0.076 for E2. However, the maximum corresponding to ultrafine particles is variable, especially for TiO_2: $(\sigma/\bar{x})_1$=1.5, whereas it is equal to 0.63 for SiO_2. This could indicate that the ultrafine aggregate generation by breakage and/or erosion of the micrometric agglomerates could be somewhat dependent on the operating conditions such as temperature or humidity which were not controlled during the experiments.

3.3.2 SEM visualisation

The presence of ultrafine aggregates in the air after the powder fall was checked by removing particles down the ELPI stages and analysing the collected particles with a scanning electron microscope (SEM). **Fig.s 10.a** to **10.c** show two ultrafine aggregates of SiO_2 and one of TiO_2 found on the 1st, the 2nd and the 3rd stage of the ELPI device, respectively.

In all cases, two main remarks can be made. The first one is that ultrafine aggregates are actually present in the aerosol, as observed from the ELPI measurements. This result shows that the peak corresponding to ultrafine particles in the size distributions given by the ELPI measurement in the chamber is representative of this population and is not due to measurement fluctuations. The second one is that aggregates and agglomerates are not spherical. This is especially the case with silica, whose aggregates seem to have a fractal structure in several cases as in **Fig. 10.a**.

3.4 Influence of the height of fall

As shown in **Fig. 8**, neither the shape of the size distribution nor the position of the maxima is modified by the height of fall. However, increasing the height of fall increases the micrometric agglomerates concentration. On the other hand, the effect of the height of fall on the ultrafine aggregates concentration is not clear due to the problems of reproducibility of the experiments. This problem is stronger when the height of fall is small (50cm, experiments E5 and E8). In this case, the peak in the raw current

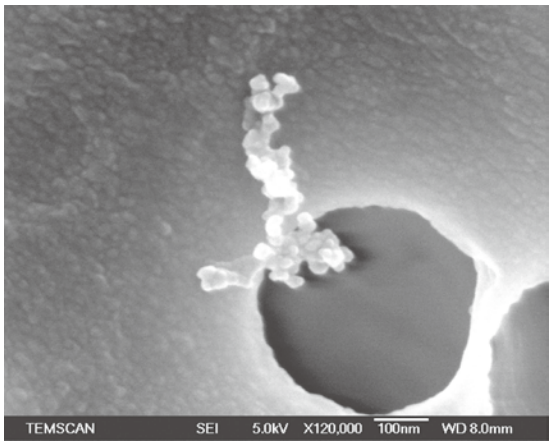

Fig. 10a SiO_2, 1st stage (×120000)

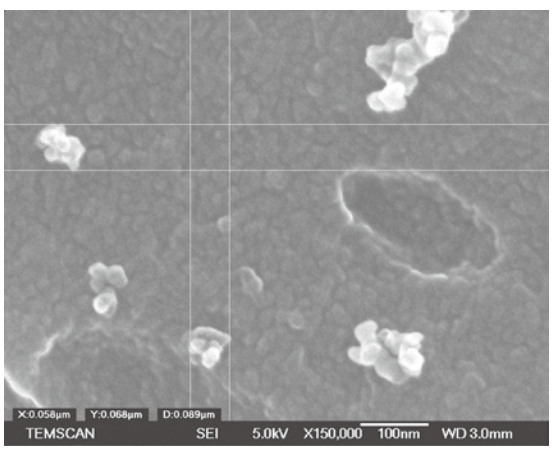

Fig. 10b SiO_2, 2nd stage (×150000)

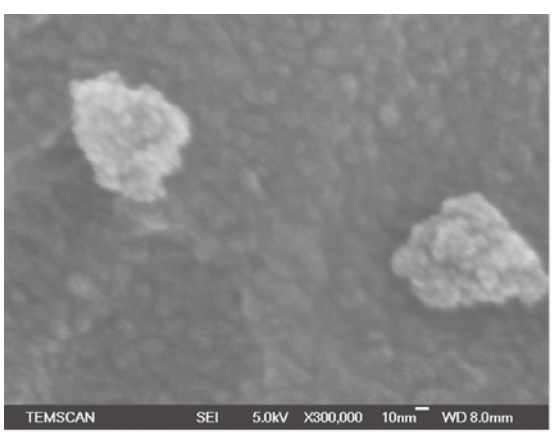

Fig. 10c TiO_2, 3rd stage (×300000)

Fig. 10 SEM visualisation of ultrafine aggregates collected on the ELPI stages.

is small and the drift of the instrument becomes too important. This leads to a larger imprecision for experiments E5 and E8 than for the others.

Fig. 11.a shows the influence of the falling height on the mass concentration of the TiO_2- and the SiO_2-generated aerosols. For the same volume of dropped powder, the dependence of mass concentration upon the falling height seems to be well described by a straight line for SiO_2, whereas for TiO_2, this dependence correlates with the square of this height. It is generally supposed in the literature[25-29] that the resuspension of micrometric particles depends upon a power of the falling height, h^{α}, where α varies from 0.4[29] to 2.05[26]. Moreover, the value of α could depend on the type of the powder. Hence, our results for both powders seem to agree with previous works on micrometric powders.

3.5 Influence of the dropped mass

One should not be tempted to directly compare the concentration of the SiO_2 aerosol in experiments E1, E3 to E5 with that of the TiO_2 aerosol in experiments E2, E6 to E8. One could induce that TiO_2 is much dustier than SiO_2. In fact, the mass of TiO_2 that falls in those experiments is 8 times higher than that of SiO_2. It seems more judicious to compare the aerosol concentrations normalised by the mass of the fall. Results are shown in **Fig. 11.b**. Although normalised mass concentrations of TiO_2 are within the confidence interval of the SiO_2 values for a confidence level of 95%, these values are always smaller than those for SiO_2. We can therefore deduce that SiO_2 is a little dustier than TiO_2.

Another way to compare the two powders is to use the same mass of falling powder in the beaker of the experiment (and not the same volume). **Fig.s 11.a** and **11.b** represent the mass concentrations for experiments E11, E12 and E13, for which the dropped mass of TiO_2 was equal to the dropped mass of SiO_2 used in E1, E3 to E5 experiments. We can see that for the same dropped mass, the SiO_2 aerosol mass concentrations are about 5 times higher than those of TiO_2 aerosols. This consolidates the affirmation that the tested SiO_2 nanopowder is dustier than the tested TiO_2 one.

Fig. 11.b shows that increasing the dropped mass increases the normalised mass concentration. When the dropped mass is reduced, the proportion of powder impacting on a layer of previously dropped particles is reduced. Since this is the main mechanism of particle release, the quantity of re-suspended particles is lower, even when normalising the mass by the dropping mass. This observation agrees with Heitbrink *et al*'s work[28].

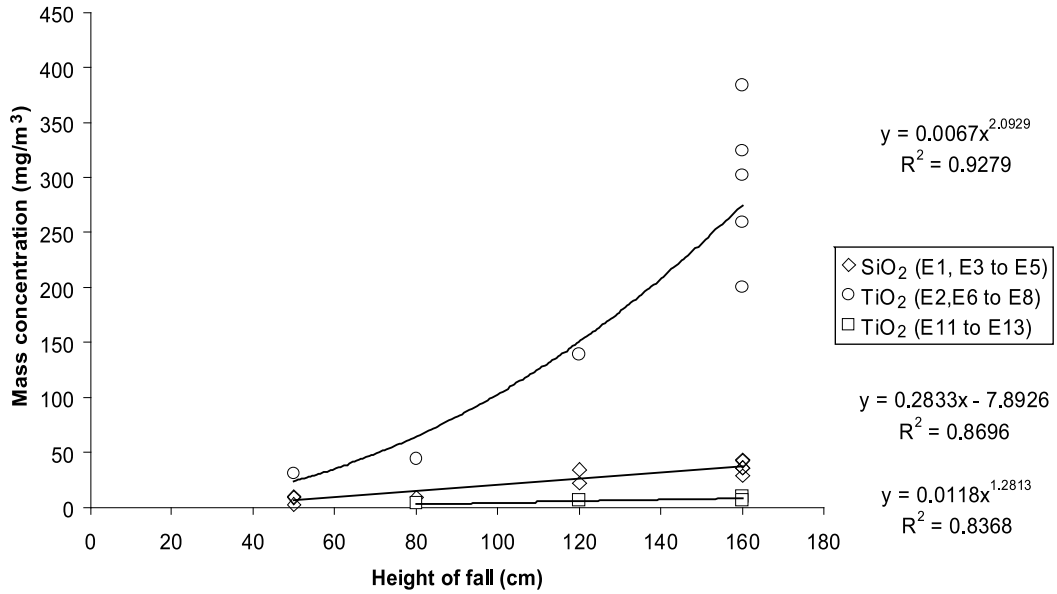

Fig. 11a Absolute values of the generated aerosol.

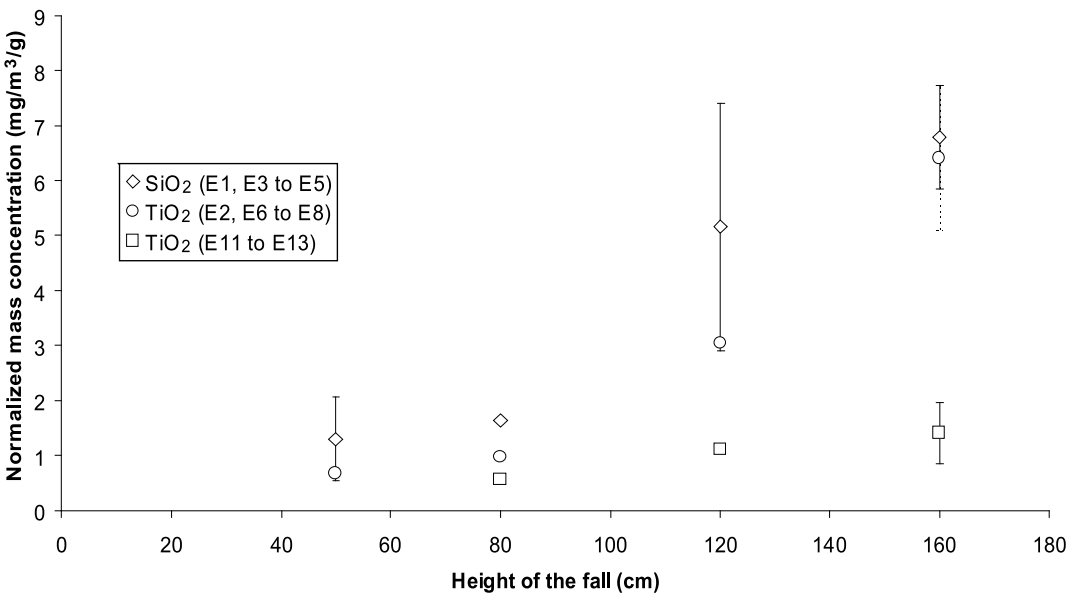

Fig. 11b Normalised values (aerosol mass concentration to the mass of the falling powder ratio).

Fig. 11 Influence of the height of fall and the dropped mass on the mass concentration of the generated aerosols.

4. Discussion

The average number of particles falling each time (n_{fall}) can be estimated from the mass of the falling powder (m_{fall}), the particle density (ρ_p) and the diameter (d_p):

$$n_{fall} = \frac{m_{fall}}{\rho_p \cdot (\pi/6) \cdot d_p^3} \quad (4)$$

By normalising the particle number concentration on the 1st ELPI stage by n_{fall}, a value of 10^{-8} part/cm^3 in the aerosol per dropped particle was obtained for SiO_2, whereas it is 10^{-11} for TiO_2 (experiments E1 and E2, respectively). Although it is a rough estimation, it is a good indication of the fact that SiO_2 agglomerates break more easily than the TiO_2 ones. The reason seems to be the much more open structure of the SiO_2 agglomerates (see **Fig. 2**).

The void fraction, ε, of TiO_2 agglomerates can be estimated from the agglomerate density ρ_{agg} (measured by helium picnometry, **Table 2**) and the primary particle density ρ_{pp}, calculated from the crystallographic parameters[30]. It is found to be equal to

0.20.

$$\varepsilon = 1 - (\rho_{agg}/\rho_{pp}) \quad (5)$$

Since fumed silica is amorphous, the void fraction must be estimated using another method. It can be calculated from their fractal dimension, D_f, Eq.(7)[31]. The average fractal dimension for SiO_2 agglomerates can be measured by laser scattering[31] with Mastersizer 2000, and it has been found to be roughly equal to 2.1; this method, however, cannot be performed with TiO_2 since TiO_2 agglomerates are too small, and very large scattering wave vectors, not available in the Mastersizer 2000, are needed[32].

The solid-fraction-to-void-fraction ratio for SiO_2 can be calculated by Eq.(6). It is found to be $4 \cdot 10^{-3}$ for SiO_2. This ratio is 1 000 times higher for TiO_2.

$$\frac{1-\varepsilon}{\varepsilon} \cong (d_{agg}/d_{pp})^{D_f-3} \quad (6)$$

If the interparticle forces are attributed to van der Waals interactions[33], then they are roughly equal for both SiO_2 and TiO_2.

$$F = \frac{A \cdot d_{pp}}{24 \cdot z^2} \quad (7)$$

Finally, the primary particle size for TiO_2 is smaller than for SiO_2 (see **Table 2**). Rumpf's theory[34] establishes that the tensile strength of an agglomerate (σ_t) depends upon its void fraction (ε), the interparticle force (F) and the primary particle size (d_{pp}):

$$\sigma_t = \frac{1-\varepsilon}{\varepsilon} \cdot \frac{F}{d_{pp}^2} \quad (8)$$

Applying Rumpf's theory, we find that the tensile strength for TiO_2 agglomerates is at least 1000 times higher than for the SiO_2 ones. This could explain why SiO_2 agglomerates break more easily than the TiO_2 ones. However, attention should be paid to the fact that the hydrodynamic stresses are not necessarily the same.

In the future, the powder fall will be simulated by an Eulerian-Lagrangian approach, in order to study the mechanism of the particle release.

Nomenclature

A	Hamaker constant	[J]
C_C	slip correction factor	[-]
d_a	aerodynamic diameter	[m]
d_{agg}	agglomerate diameter	[m]
d_b	mobility diameter	[m]
d_p	particle diameter	[m]
d_{pp}	primary particle diameter	[m]
E_{ch}	charger efficiency	[A/m3]
F	interparticle force	[N]
h	falling height	[m]
I	measured current	[A]
I'	corrected current	[A]
m_{fall}	mass of powder falling	[kg]
N	particle number concentration in the air	[particles/m^3]
n_{fall}	number of particles falling	[-]
$\bar{x}_i$	average of the particle number concentration corresponding to the ith ELPI stage	[particles/m^3]
z	interparticle distance	[m]
ε	void fraction of an agglomerate	[-]
ρ_0	unit density: 1000 kg/m^3	
ρ_{agg}	agglomerate density	[kg/m^3]
ρ_p	particle density	[kg/m^3]
ρ_{pp}	primary particle density	[kg/m^3]
σ_i	standard deviation of the particle count concentration on the ith ELPI stage	[particles/m^3]
σ_t	tensile strength of an agglomerate	[N/m^2]

Acknowledgements

The authors acknowledge the CNRS, Centre National de Recherche Scientifique and the INRS, Institut National de Recherche et Securite for their financial support within the frame of the DINANO project. They also want to acknowledge Lucien Datas and Stéphane Le Blond du Plouy from the TEMSCAN Service of the University of Toulouse for the SEM and the TEM visualisations.

References

1) Brune, H., Ernst, H., Grünwald, A., Grunwald, W., Hofmann, H., Krug, H., Janich, P., Mayor, M., Rathgeber, W., Schmid, G., Simon, U., Vogel, V., Wyrwa, D.: Nanotechnology. Assessment and Perspectives. Springer Berlin Heidelberg, 2006.
2) Aitken, R.J., Creely, K.S., Tran, C.L.: Nanoparticles: An occupational hygiene review. Research Report 274. Health and Safety Executive (HSE) UK, 2004.
3) Maynard, A D., Kuempel, E.D.: Airborne nanostructured particles and occupational health. J. Nanopart. Res. 7, 2005, 587-614.
4) Maynard, A.D. Nanotechnology: assessing the risks. Nanotoday 1, 2006, 22-33.
5) Oberdörster, G., Ferin, R., Gelein, J., Soderholm, S.C., Finkelstein, J.: Role of the alveolar macrophage in lung injury – studies with ultrafine particles. Environ. Health Persp. 97, 1992, 193-199.
6) Oberdörster, G., Sharp, Z., Atudorei, V., Elder, A., Gelein, R., Lunts, A., Kreyling, W., Cox, C.: Extrapulmonary translocation of ultrafine carbon particles following wholebody inhalation exposure of rats. J. Toxicol. Environ. Health Part A, 65, 2002, 1531-1543.
7) Duffin, R., Tran, C.L., Clouter, A., Brown, D.M., MacNee, W., Stone, V., Donaldson, K.: The importance of

surface area and specific reactivity in the acute pulmonary inflammatory response to particles. Ann. Occup. Hyg. 46, 2002, 242-245.
8) Hamelmann, F., Schmidt, E.: Methods for Estimating the Dustiness of Industrial Powders – A review. Kona 21, 2003, 7-18.
9) Baron, P.A., Maynard, A.D., Foley, M.: Evaluation of Aerosol Release During the Handling of Unrefined Single Walled Carbon Nanotube Material. NIOSH DART-02-191, 2003.
10) Maynard, A.D., Baron, P.A., Foley, M., Shvedova, A.A., Kisin, E.R., Castranova, V.: Exposure to carbon nanotube material: aerosol release during the handling of unrefined single-walled carbon nanotube material. J. Toxicol. Environ. Health Part A 67, 2004, 87-107.
11) Hamelmann, F., Schmidt, E.: Methods for Characterizing the Dustiness Estimation of Powders. Chem. Eng. Technol. 27, 2004, 844-847.
12) Flagan, R.C.: Electrical Techniques, in: Baron, P.A., Willeke, K. eds: Aerosol Measurement. Principles, Techniques, and Applications. 2nd ed. John Wiley & Sons, 2001.
13) Baron, P.A., Mazumder, M.K., Cheng, Y.-S.: Direct-Reading Techniques Using Particle Motion and Optical Detection, in: Baron, P.A., Willeke, K. eds: Aerosol Measurement. Principles, Techniques, and Applications. 2nd ed. John Wiley & Sons, 2001.
14) Cowherd, C.jr., Grelinger, M.A., Englehart, P.J., Kente, R.F., Wong, K.F.: An Apparatus and Methodology for Predicting the Dustiness of Materials. Am. Ind. Hyg. Assoc. J. 50, 1989, 123-130.
15) Keskinen, J., Pietarinen, K., Lehtimaki, M.: Electrical Low Pressure Impactor. J. Aerosol Sci. 23, 1992, 353-360.
16) Marjamäki, M., Keskinen, J., Chen D.-R., Pui, D.Y.H.: Performance evaluation of the Electrical Low-Pressure Impactor (ELPI). J. Aerosol Sci. 31, 2000, 249-261.
17) Moisio, M.: Real Time Size Distribution Measurement of Combustion Aerosols. PhD Thesis. Tampere University of Technology, 1999.
18) Dekati Ltd.: ELPI user manual ver 3.20, 2003.
19) Dekati Ltd.: Elpivi 3.1 Software Manual ver 3.20, 2003.
20) Virtanen, A., Marjamäki, M., Ristimäki, J., Keskinen, J.: Fine particle losses in electrical low-pressure impactor. J. Aerosol Sci. 32, 2001, 389-401.
21) Marjamäki, M., Lemmety, M., Keskinen, J.: ELPI Response and Data Reduction I: Response Functions. Aerosol Sci. Technol. 39, 2005, 575-582.
22) Baltensperger, U., Weingartner, E., Burtscher, H., Keskinen, J.: Dynamic Mass and Surface Area Measurements, in: Baron, P.A., Willeke, K. eds: Aerosol Measurement. Principles, Techniques, and Applications. 2nd ed. John Wiley & Sons, 2001.
23) Hinds, W.C.: Aerosol Technology. Properties, Behavior, and Measurement of Airborne Particles. 2nd ed. John Wiley & Sons, 1999.
24) Uchiyama, T., Naruse, M. Three-dimensional vortex simulation for particulate jet generated by free falling particles. Chem. Eng. Sci. 61, 2006, 1913-1921.
25) Cheng, L.: Formation of Airborne Respirable Dust at Belt Conveyor Transfer Points. Am. Ind. Hyg. Assoc. J. 34, 1973, 540-546.
26) Sutter, S.L., Johnston, J.W., Mishima, J.: Investigation of Accident-Generated Aerosols: Releases from Free Fall Spills. Am. Ind. Hyg. Assoc. J. 43, 1982, 540-543.
27) Plinke, M.A.E., Leith, D., Holstein, D.B., Boundy, M.G. Experimental Examination of Factors That Affect Dust Generation. Am. Ind. Hyg. Assoc. J. 52, 1991, 521-528.
28) Heitbrink, W.A., Baron, P.A., Willeke, K. An Investigation of Dust Generation by Free Falling Powders. Am. Ind. Hyg. Assoc. J. 53, 1992, 617-624.
29) Plinke, M.A.E., Leith, D., Boundy, M.G., Löffler, F. Dust Generation from Handling Powders in Industry. Am. Ind. Hyg. Assoc. J. 58, 1995, 251-257.
30) www.mindat.org/min-213.html
31) Wengeler, R., Nirschl, H.: Turbulent hydrodynamic stress induced dispersion and fragmentation of nanoscale agglomerates. J Colloid Interf. Sci. 306, 2007, 262-273.
32) Sorensen, C.M.: Light Scattering by Fractal Aggregates: A Review. Aerosol Sci. Technol. 35, 2001, 648-687.
33) Israelachvili, J. Intermolecular and Surface Forces, 2nd ed. Academic Press, 1992.
34) Reynolds, G.K., Fu, J.S., Cheong, Y.S., Hounslow, M.J., Salman, A.D.: Breakage in granulation: A review. Chem. Eng. Sci. 60, 2005, 3969-3992.

Author's short biography

Nelson Ibaseta

Nelson Ibaseta obtained his B.Eng. degree in chemical engineering from the University of Oviedo, Spain, and his M.Sc. degree in chemical and environmental engineering from the National Polytechnic Institute of Toulouse, France, where he is currently working on his Ph.D. thesis. His research interests are in multiphase systems, ranging from physicochemical and transfer systems to simulation and optimisation aspects.

Béatrice Biscans

Dr Béatrice Biscans is a permanent researcher at CNRS (French National Centre for Scientific Research), in the Chemical Engineering Laboratory in Toulouse, in charge of a group working on crystallisation and nanoparticles. Her research interests are directed towards understanding and predicting the properties of solid-form chemical products through control of the process parameters. She develops both theoretical and experimental studies associated with both fundamental and strategic research programmes including industrial collaboration.